ACS OMEGA

http://pubs.acs.org/journal/acsodf

Article

Facile Synthesis of Vanadium Oxide/Carbon Spheres-Doped Nickel Oxide Functioned as a Nanocatalyst and Bactericidal Behavior with Molecular Docking Analysis

Shair Baz, Muhammad Ikram,* Ali Haider, Anum Shahzadi, Anwar Ul-Hamid,* Walid Nabgan,* Junaid Haider, M. Imran, Thamraa Alshahrani, Francisco Medina, and Muhammad Imran

Cite This: *ACS Omega* 2023, 8, 19474−19485

Read Online

ACCESS | Metrics & More | Article Recommendations

ABSTRACT: Vanadium oxide (V_2O_5) and carbon spheres (Cs)-doped NiO_2 nanostructures (NSs) were prepared using the co-precipitation approach. Several spectroscopic and microscopic techniques, including X-ray diffraction (XRD), UV−vis, FTIR, TEM, and HR-TEM investigations, were used to describe the as-synthesized NSs. The XRD pattern exhibited the hexagonal structure, and the crystallite size of pristine and doped NSs was calculated as 29.3, 32.8, 25.79, and 45.19 nm, respectively. The control sample (NiO_2) showed maximum absorption at 330 nm, and upon doping, a redshift was observed, leading to decreased band gap energy from 3.75 to 3.59 eV. TEM of NiO_2 shows agglomerated nonuniform nanorods exhibited with various nanoparticles without a specific orientation; a higher agglomeration was observed upon doping. The (4 wt %) V_2O_5/Cs-doped NiO_2 NSs served as superior catalysts with a 94.21% MB reduction in acidic media. The significant antibacterial efficacy was estimated against *Escherichia coli* by measuring the zone of inhibition (3.75 mm). Besides their bactericidal analysis, V_2O_5/Cs-doped NiO_2 was shown to have a binding score of 6.37 for dihydrofolate reductase and a binding score of 4.31 for dihydropteroate synthase in an in silico docking study of *E. coli*.

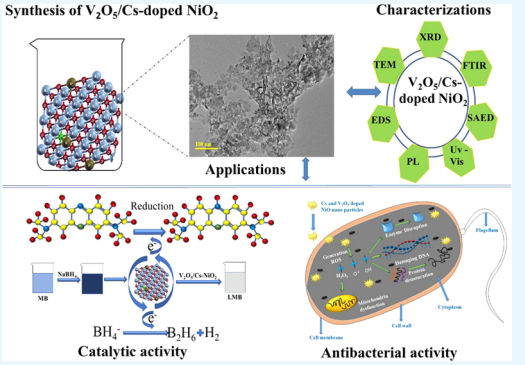

1. INTRODUCTION

Rapid growth in population, chemical fertilizers, industrialization, and increased urban wastewater outputs have revealed the most significant environmental issues.[1] The primary contaminants in polluted water are waste from several industries, including paper, plastic, leather, food, textile sectors, and organic dyes.[2] The most frequently employed cationic dye in industries is methylene blue (MB). The primary adverse effects of this harmful dye in humans include respiratory irritation, teratogenicity, and carcinogenicity.[3−5] The dye pollutants are often cleaned using various physical, biological, and chemical techniques such as catalysis, flocculation, absorption, aeration, and photooxidation.[6−8] Among them, the dye is broken down by a catalytic process, while nanomaterials are present that are relatively simple, cost-effective, and eco-friendly.[6]

Metal oxides (MOs) have gained much attention in the catalysis process attributed to their minimal toxicity, high chemical stability, inexpensive, and environmentally favorable qualities.[6] MOs have significant adsorption and catalytic properties as well as reactivity and sorption capacity assigned to their large specific surface area and small size. According to the literature, a number of prepared MOs,[9] such as La_2O_3,[10] Er_2O_3,[11] Tm_2O_3,[12] and Y_2O_3,[13] are considered chemically stable and toxic and have broad band gaps (∼4.3−7 eV). On the other hand, nickel oxide (NiO_2) is a feasible alternative since it is commonly accessible, inexpensive, and electrochemically stable, with a minimal band gap of 3.6−4.0 eV.[14] Furthermore, the catalytic abilities and chemical stability of NiO_2 can be enhanced by suitable dopants.[15]

In recent studies, many polymers have been used as dopants for the reduction of MB, such as polyvinylpyrrolidone, polyaniline, polydopamine, poly(*N*-vinylcaprolactam), and carbon spheres (Cs).[16−20] Many researchers used chitosan, cellulose nanocrystal, and poly(acrylic acid) in the MO that degraded MB 88% for 220 min, 70.6% after 30 min, and 65% in 60 min, respectively.[21−23] The above-mentioned catalysts/photocatalysts have some drawbacks such as a low photoresponse toward visible light, high cost, and longer reduction time. Among them, Cs is a potential contender in the realm of catalysis due to the availability of various surface functional

Received: February 7, 2023
Accepted: May 8, 2023
Published: May 22, 2023

groups (such as carbonyl, hydroxyl, and carboxylic) with a high specific surface area, superior chemical durability, and high biocompatibility.[24,25] Furthermore, V_2O_5 has excellent redox properties and can be used as a co-catalyst. It has a 3d3-4s2 valence electron layer structure with a remarkable stability, a large surface area, a high energy density, and a high conductivity.[26−28]

Most of these above-reported catalysts/photocatalysts are related to limitations such as the low photoresponse toward visible light, high cost, and longer degradation time. The proposed material (2 and 4 wt %) V_2O_5/Cs-doped NiO_2 nanostructures (NSs) would be the best candidate for catalytic and antimicrobial activities. The potential of this work is that Cs have a wide surface area and porous structure and promote NiO_2 adsorption and reaction, which can improve contact between the NiO_2 and the microbes, resulting in a more effective antimicrobial and catalytic activity. Furthermore, adding V_2O_5 into Cs-doped NiO_2 can improve its catalytic and antimicrobial activity by increasing the availability of reactive oxygen species (ROS) and boosting redox reactions. The pathogen *Escherichia coli*, which broadly spreads through contaminated water and causes diarrhea, kills 1.3 million children globally yearly.[29] In this regard, NSs that are tiny, mobile, and conductive prevent bacterial adherence.[30,31]

The co-precipitation approach has been employed in this study to synthesize V_2O_5/Cs-doped NiO_2 NSs. Characterizations were carried out utilizing techniques such as XRD, FTIR, TEM, HR-TEM, UV−vis, and PL for a detailed study. The prepared ternary system composite can remove organic dyes like MB. Furthermore, their antibacterial experiments against *E. coli* (Gram-negative) bacteria were carried out through the agar well diffusion method, and the binding propensity of NSs was investigated using molecular docking predictions.

2. EXPERIMENTAL SECTION

2.1. Materials. Nickel nitrate hexahydrate [$Ni(NO_3)_2 \cdot 6H_2O$, 98%] has been purchased from VWR Chemicals, and NaOH glucose and V_2O_5 were obtained from Sigma-Aldrich (Germany). The entire chemicals were in pure form and used without any further purification.

2.2. Synthesis. *2.2.1. Preparation of Cs.* The Cs have been synthesized using a hydrothermal carbonization method. Initially, 1 M glucose solution was diluted under steady stirring to achieve a clear and transparent solution. The colloidal solution was placed in a stainless autoclave at 180 °C for 12 h. The obtained precipitates were washed several times using deionized (DI) water and dried overnight at 100 °C (Figure 1a).

2.2.2. Synthesis of V_2O_5/Cs-Doped NiO_2. NiO_2 was prepared through a chemical co-precipitation route using $Ni(NO_3)_2 \cdot 6H_2O$ as a precursor under continuous stirring at 100 °C. After 30 min, 1 M NaOH was incorporated to maintain pH ≈ 12 and to obtain precipitates. Furthermore, the obtained precipitates have been washed through centrifugation at 7000 rpm for 7 min several times. The washed precipitates were dried at 150 °C for 12 h to sustain the fine powder. The same procedure was carried out to prepare a fixed amount of Cs and different concentrations (2 and 4 wt %) of V_2O_5-doped NiO_2 (Figure 1b).

2.3. Catalytic Activity. The catalytic activity (CA) of NiO_2 and (2 and 4 wt %) V_2O_5/Cs-doped NiO_2 NSs for MB reduction was investigated in sodium borohydride ($NaBH_4$).

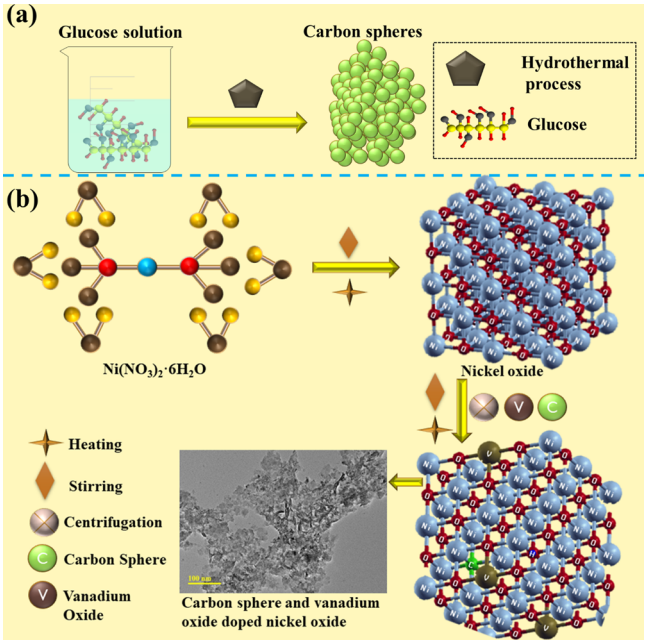

Figure 1. (a, b) Schematic illustration of Cs and V_2O_5/Cs-doped NiO_2 synthesis.

MB and $NaBH_4$ solutions were prepared freshly to perform CA, and 400 μL of $NaBH_4$ was incorporated into the MB solution to check the %age reduction. Afterward, the freshly prepared nanocatalyst solution (400 μL) was introduced into the above solution, and MB color started to change into its leuco form. As a direct result, a UV−vis spectrophotometer was employed to obtain consistent recordings of the absorption variation spectra. A formula was used to calculate the percentage of degradation:

$$\%\text{degradation} = (C_o - C_t)/C_o \times 100$$

where C_o is the initial concentration of MB dye solution and C_t is the specific time concentration after incorporating NSs.

2.4. Isolation and Identification of MDR *E. coli*. *2.4.1. Isolation of E. coli. 2.4.1.1. Sample Collection.* Raw milk samples have been gathered from the veterinary form sold at different markets, veterinary clinics, and farms in Punjab, Pakistan. The milk was then directly poured into sterile glassware. Raw milk was gathered at 4 °C and transported to the lab immediately. Coliforms discovered in raw milk were enumerated on MacConkey agar. All plates were kept in an incubator for 48 h at 37 °C.

2.4.2. Identification and Characterization of Bacterial Isolates. Initial recognition of *E. coli* was based on the colonial structure by Gram stain and by numerous biochemical investigations with reverence to Bergey's Manual of Determinative Bacteriology *E. coli*.[32]

2.4.2.1. Antibiotic Susceptibility. To determine the antibiotic susceptibility of the sample, the agar well diffusion method was used, which was carried out on Mueller−Hinton agar (MHA).[33] The antimicrobial tests were conducted to investigate the *E. coli*'s resistance to antimicrobial classes such as cephalosporins (ceftriaxone (Cro) 30 μg), aminoglycosides (gentamicin (Gm) 10 μg), quinolones (ciprofloxacin (Cip) 5 μg), carbapenems (imipenem (Imi) 10 μg), penicillins (amoxicillin (A) 30 μg), tetracyclines (tetracycline (Te) 30 μg), and macrolides (azithromycin (Azm) 15 μg).[34] Following

https://doi.org/10.1021/acsomega.3c00604
ACS Omega 2023, 8, 19474−19485

the McFarland standard, a turbidity level of 0.5 was attained by growing pure *E. coli* cultures. The bacteria were distributed throughout MHA (Oxoid Limited, Basingstoke, United Kingdom), and antibiotic discs were subsequently positioned at a distance on the surface of the inoculation plate. This was done to prevent interfering with inhibitory zones. The plates were incubated for 48 h at 37 °C, and the data were examined by Diagnostic and Laboratory Standard Institute instructions.[35] Bacteria resistant to at least three antibiotics were proclaimed MDR.[36]

2.4.2.2. Antimicrobial Activity. A good diffusion test evaluated the microbicidal performance of the pure (2 and 4 wt %) V_2O_5/Cs-doped NiO_2 NSs against pathogenic *E. coli*. MacConkey agar was treated with MDR *E. coli* at a concentration of 1.5×10^8 CFU/mL (0.5 McFarland standard). To examine the bactericidal capability of pristine and doped NSs, *E. coli* infection bacteria were successfully isolated from ovine mastitis milk. On MacConkey agar and mannitol salt plates that had been cleaned with 0.5 McFarland of *E. coli*, piercing wells with an internal diameter of approximately 6 mm were punctured using a sterilized borer. The conventional antibiotic ciprofloxacin (5 mg/50 μL) was employed as a positive control, while 50 μL of DI water functioned as a negative control. After that, the boreholes were filled with pristine and doped NSs at high and low concentrations (1.0 mg/50 μL and 0.5 mg/50 μL), respectively.[37] Then, the plates were contaminated aerobically for 12 h at 37 °C, and the inhibited zones around the surroundings of the wellbores were determined utilizing a vernier caliper to determine the antimicrobial properties.

2.4.2.3. Statistical Analysis. Zones of inhibition were used to assess antimicrobial performance and their diameters were subjected to statistical analysis using one-way analysis of variance (ANOVA) in SPSS 20.[38]

2.5. Molecular Docking Study. *2.5.1. Method.* The proposed mode of action for V_2O_5/Cs-doped NiO_2 has been predicted using in silico docking, a potential method for determining the distinctive structural characteristic underpinning microbicidal activity. Dihydrofolate reductase (DHFR) and dihydropteroate synthase (DHPS), two essential enzymes in folate biosynthesis, have been singled out as promising antibiotic targets. The three-dimensional structures of target enzymes were obtained from the Data Bank of Protein and then created using a protein synthesis tool to facilitate the docking of V_2O_5/Cs-doped NiO_2 into the active site. Preferred targets were tagged with the annexation codes 2ANQ ($DHFR_{E.coli}$)[39] and 5U0V ($DHPS_{E.coli}$).[40] The SYBYL-X 2.0 program was used for the docking investigation. As in our previous work,[41,42] we used SYBYL-X 2.0 to model compounds in three dimensions and evaluated nanoparticle binding affinities with the residues found in the active sites of certain proteins.

3. RESULTS AND DISCUSSION

The phase composition and structural characteristics of prepared NiO_2 and (2 and 4 wt %) V_2O_5/Cs-doped NiO_2 NSs were examined using XRD, ranging between 2θ = 20 and 80° (Figure 2a). Diffraction peaks sited at 33.0, 38.5, 52.0, 59.0, 62.6, and 72.8° associated with crystal planes (010), (011), (012), (110), (111), (020), and (112), respectively, well matched with JCPDS card 96-901-1315, having a hexagonal crystal structure and space group *p*-3*m*1. The XRD patterns showed no extra peak, confirming the formation

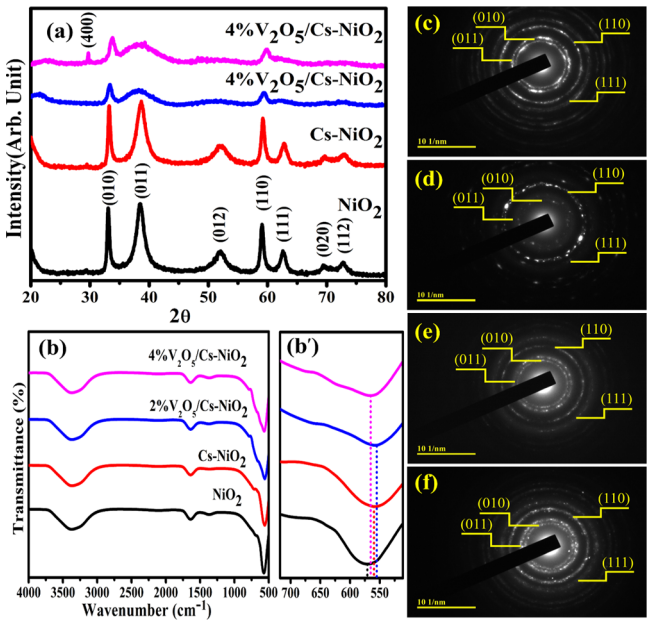

Figure 2. (a) XRD pattern of NSs, (b) FTIR spectra of NSs, (b′) zoom area of the Ni−O band, and SAED pattern of (c) NiO_2, (d) Cs-doped NiO_2, (e) (2 wt %) V_2O_5/Cs-doped NiO_2, and (f) (4 wt %) V_2O_5/Cs-doped NiO_2.

of single-phase NiO_2. An XRD spectrum of 4 wt % showed an additional diffraction peak of V_2O_5 at 29.5° (400).[43] This result indicates that the doping of V_2O_5 with low concentrations has a minor effect on the phase structure.[44] Consequently, the peaks were shifted toward higher 2θ values, suggesting that the Cs is present in the pristine matrix and filling the void between Ni and O. The XRD peaks shift toward a higher angle corresponding with interstitial site doping.[45] In addition, crystalline defects, lattice deformation, domain size dispersion, and crystalline domain size cause peak broadness in the doped samples.[46] The peak intensity was diminished upon doping V_2O_5 compared to the pristine and Cs-doped NiO_2. The crystallite size from the most instance peak (010) for pure and doped NiO_2 NSs was measured using the Debye−Scherrer formula as 29.3, 32.8, 25.79, and 45.19 nm.

FTIR spectroscopy used to identify the functional groups (4000 to 1500 cm^{-1}) and the fingerprint regions (1500 to 400 cm^{-1}) on the surfaces of NSs are shown in Figure 2b.[47] The O−H stretching vibration causes the broad and intense band at 3373 cm^{-1}. Furthermore, the band observed at 1648 cm^{-1} were assigned to the bending and stretching vibrations of the −OH group absorbed on the catalyst surface during the FTIR measurement.[48] The peak at 1368 cm^{-1} probably refers to some leftovers of the precursor elements utilized to prepare the NiO_2.[49] Ni−O bonds are responsible for absorption peaks beneath 1000 cm^{-1}.[50] The sharp band at 570 cm^{-1} was caused by the Ni−O stretching vibrations.[51] Upon doping of Cs and V_2O_5, peaks were shifted toward a lower wavenumber (Figure 2b′). The blue shift of doped and NiO_2 NSs was linked to the quantum size effect and the NSs.[52] The SAED images used to identify the polycrystalline nature of synthesized pristine and doped NiO_2 NSs are shown in Figure 2c−f. Images containing concentric rings that are polycrystalline were categorized as planes (101), (011), (110), and (111), which agree with the XRD results, confirming the crystalline nature of controlled and doped NiO_2.

https://doi.org/10.1021/acsomega.3c00604
ACS Omega 2023, 8, 19474−19485

To investigate the optical absorption properties of pristine and (2 and 4 wt %) V_2O_5/Cs-doped NiO_2 NSs, a UV−vis spectrophotometer was used (Figure 3a). The significant

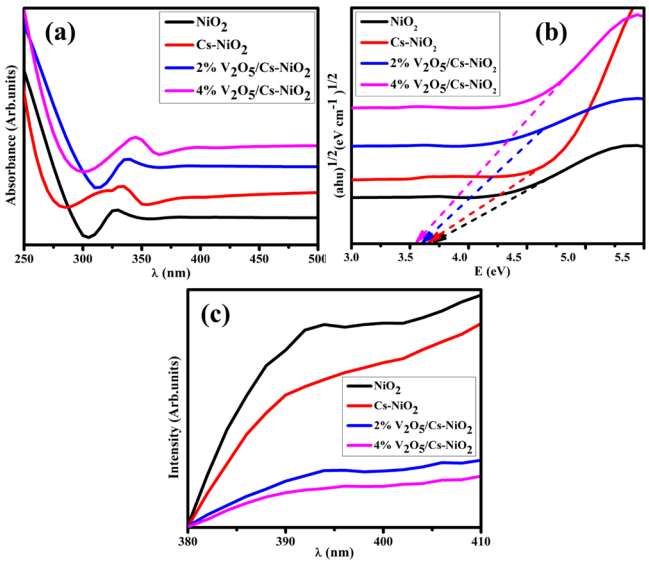

Figure 3. (a) Optical absorption spectra, (b) band gap energy, and (c) PL spectra of pure and doped NSs.

absorption bands at 330 nm for the pure NiO_2 correspond to a band gap energy of 3.75 eV determined from Tauc's plot approach.[14] Optical absorption can be affected by a wide variety of parameters, including the size of the particles and the energy gap. An electronic transition can occur from the valence band to the conduction band in the transition from O (2p) to Ni (3d) in NiO_2, resulting in a broad band at 330 nm.[53,54] The corresponding peak exhibits the symmetric forbidden transition associated with the electron injection from n to π^* transitions. The absorption maxima (λ_{max}) for Cs-NiO_2 and (2 and 4 wt %) V_2O_5/Cs-doped NiO_2 have been measured at 335, 340, and 345 nm, respectively. Figure 3a depicts that the absorption wavelength range increased with dopants introducing a redshift. The measured band gap energy values decreased gradually from 3.75 to 3.59 eV attributed to an increase in the crystalline size of NSs after doping (Figure 3b), as described earlier.

PL spectroscopy has been used to assess the photogenerated electron−hole recombination capability and separation efficiency. The PL emission spectra of undoped and (2 and 4 wt %) V_2O_5/Cs-doped NiO_2 with a range of 380−410 nm are represented in Figure 3c. The PL emission spectra of the synthesized NSs exhibit a significant peak at 393 nm[55] with an excitation wavelength of 290 nm at 37 °C. The reduction in peak intensity was found with increased dopants attributed to the difference in the ionic radii.[56] As reported, the high-intensity peak of PL confirmed a higher recombination rate of e^-−h^+ and vice versa.[57,58] The green shift was observed as the electron−hole recombination decreased, which boosted the CA.[59]

The elemental composition of NiO_2 and (2 and 4 wt %) V_2O_5/Cs-doped NiO_2 NSs was observed by EDS analysis, as presented in Figure 4a−d. Furthermore, EDS assesses the elemental distribution pattern to determine whether there is additional interfacial contact. Strong nickel and oxygen peaks were found, confirming the presence of NiO_2 in the produced samples (Figure 4a). A minor peak of sodium was observed caused by NaOH to maintain the pH of the samples. The elemental components of nickel (Ni), vanadium (V), sodium (Na), and oxygen (O) were confirmed in the doped material. On the other hand, the appearance of cesium peaks is linked to the experimental equipment and sample preparation.[60]

The elemental mapping of (4 wt %) V_2O_5/Cs-doped NiO_2 NSs is represented in Figure 5a. The existence of O, Na, V, and Ni for forming pristine and doped NiO_2 NSs is confirmed by Figure 5b−e, respectively. The presence of Na was attributed to $NaBH_4$, which was used to maintain the pH, as already mentioned.

TEM confirmed the morphologies of pristine and (2 and 4 wt %) V_2O_5/Cs-doped NiO_2, as shown in Figure 6a−d. The morphology of NiO_2 (Figure 6a) looks like agglomerated nonuniform nanorods with nanoparticles that might partially interact in a multitude of orientations. In contrast, the doping of a fixed amount of Cs into NiO_2 caused the production of the sphere, which overlaps the nanorods, indicating a reduction in the size (Figure 6b). The addition of V_2O_5 (2 and 4 wt %) to the binary system Cs-NiO_2 resulted in highly agglomerated and chunk-like morphology (Figure 6c,d). A higher degree of aggregation was observed with increasing amounts of dopants.

The interlayer d-spacing of the synthesized NiO_2 and the V_2O_5/Cs-doped NSs was measured with HR-TEM, and the results are displayed in Figure 7a−d. The interlayer d-spacing of the NiO_2 is about 0.178 nm (Figure 7a). Furthermore, the addition of Cs and (2 and 4 wt %) V_2O_5 showed considerable interplanar spacings of 0.147, 0.147, and 0.154 nm, respectively, as indicated in Figure 7b−d. The d-spacing that was predicted for pure and doped NiO_2 matched the XRD findings as well.

The CA of pristine and (2 and 4 wt %) V_2O_5/Cs-doped NiO_2 NSs was examined using a UV−vis spectrophotometer in the spectral range of 200−800 nm at various pH levels (neutral, basic, and acidic media). Various pH levels of the dye sludge are regularly released from several industries in fresh water resources. The pH of solution influences the reduction pace and impacts the artificial nanocatalyst. The CA of synthesized samples was affected by the microstructure of the materials, specifically their crystal structures, particle sizes, morphologies, and surface areas. Additionally, the OH^- and H^+ ions play critical roles in PCA and CA, respectively, and provide more OH^- radicals available to decompose the contaminant.

In the catalysis mechanism, the addition of a nanocatalyst and $NaBH_4$ that act as reducing agents to the dye is the most significant factor in the catalytic process (Figure 8). The reducing agent donates an electron to the ongoing reaction, and MB, also called the oxidizing agent, accepts an e^- from the reducing agent to carry out its role. During CA, a redox reaction starts in which an electron is transferred from the donor to the acceptor atoms. This leads to the absorption of electrons in MB, which eventually stimulates the synthetic dye to deteriorate. Additionally, MB was tested in the presence of $NaBH_4$, and the oxidation reaction was very slow. Incorporating a nanocatalyst (V_2O_5/Cs-doped NiO_2) into the oxidation−reduction reactions serves as an electron relay and makes it possible for electrons to be transferred from the donor (BH_4^-) to the acceptor (MB). NSs enhance the adsorption of BH_4^- ions and the dye molecule by providing more active sites that accelerate their interaction.[61,62] The coexistence of a nanocatalyst and a reducing agent enhances the efficiency of

https://doi.org/10.1021/acsomega.3c00604
ACS Omega 2023, 8, 19474−19485

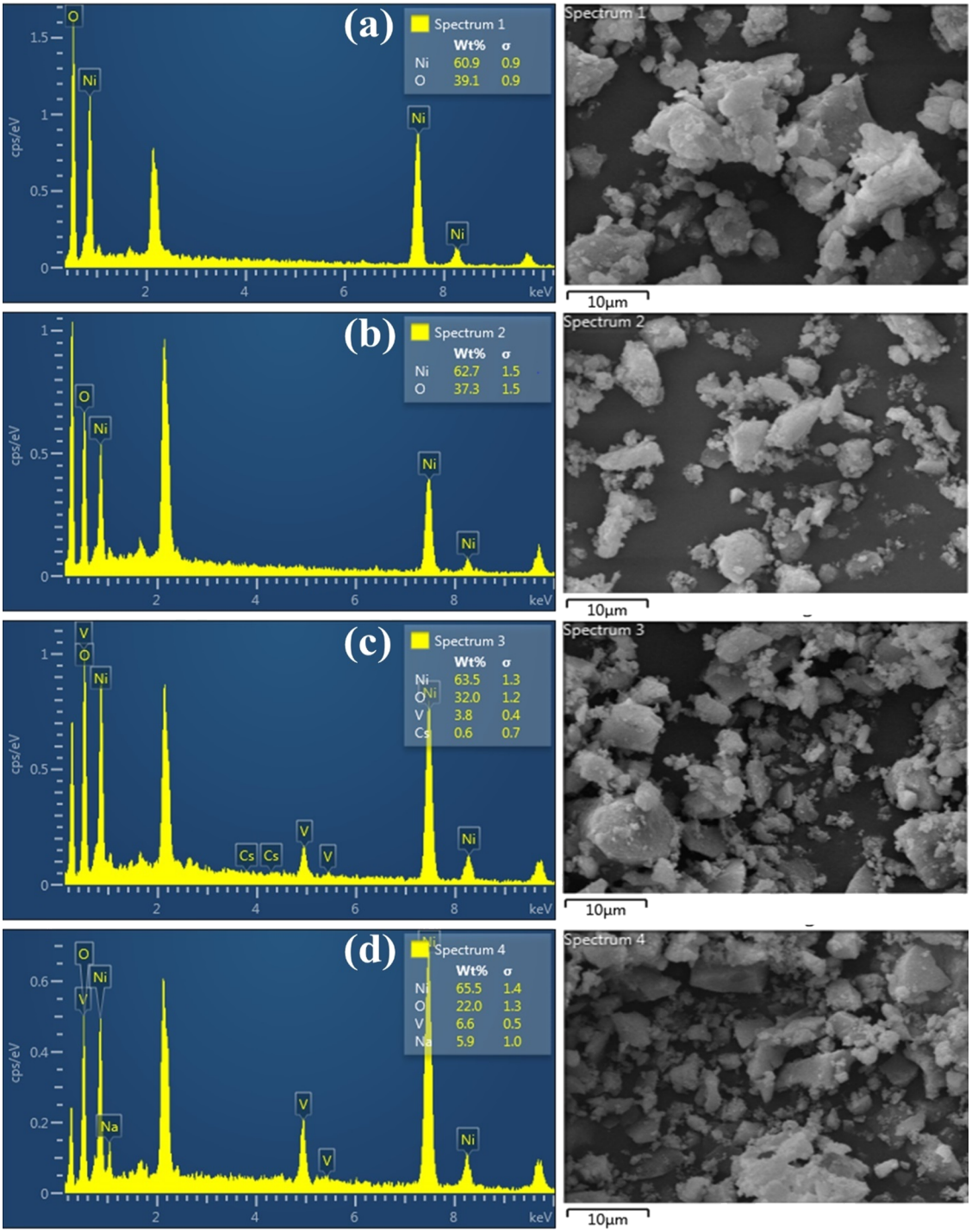

Figure 4. EDS analysis of (a) NiO_2, (b) Cs-NiO_2, (c) (2 wt %) V_2O_5/Cs-doped NiO_2, and (d) (4 wt %) V_2O_5/Cs-doped NiO_2 NSs.

degradation.[63] As NSs have a high surface-to-volume ratio, facilitating effective dye reduction, their size is another factor influencing the CA.[64]

The V_2O_5/Cs-NiO_2 NPs showed outstanding catalytic performance for the reduction of MB dye in the presence of the reducing agent $NaBH_4$, and the findings demonstrate that it exhibited the degradation of MB dye up to 75.13, 81.54, 85.76, and 91.89% in neutral (pH = 7), 59.29, 79.45, 84.22, and 91.01% in basic (pH = 12), and 63.35, 76.1, 87.37, and 94.21% in acidic (pH = 4) media, as seen in Figure 9a−c. The addition of V_2O_5 improved the CA up to 94.21%, given the ideal level for the reduction of dye exhibited by (4 wt %) V_2O_5/Cs-NiO_2. The literature review and the current experiment study for the reduction of MB can be seen in Table 1. Significant CA against MB dye was observed upon the higher incorporation of catalysts. The comparison study indicates that the recent work has maximum potential against dye reduction. However, their high electrical efficiency was attributed to encouraging the results at acidic pH for (4 wt %) V_2O_5/Cs-doped NiO_2 NSs. The excellent CA in acidic media was ascribed to the enhanced availability of hydrogen (H^+) ions for absorption on the NSs horizon.[62]

https://doi.org/10.1021/acsomega.3c00604
ACS Omega 2023, 8, 19474−19485

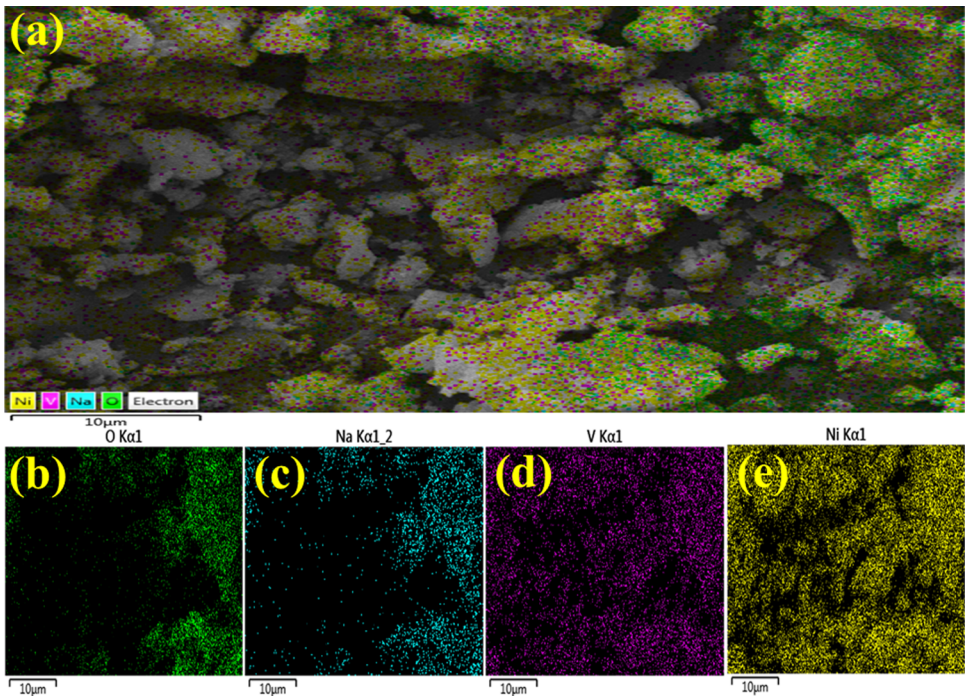

Figure 5. Elemental mapping composition of the synthesized NSs: (a) (4 wt %) V_2O_5/Cs-doped NiO_2, (b) oxygen, (c) sodium, (d) vanadium, and (e) nickel.

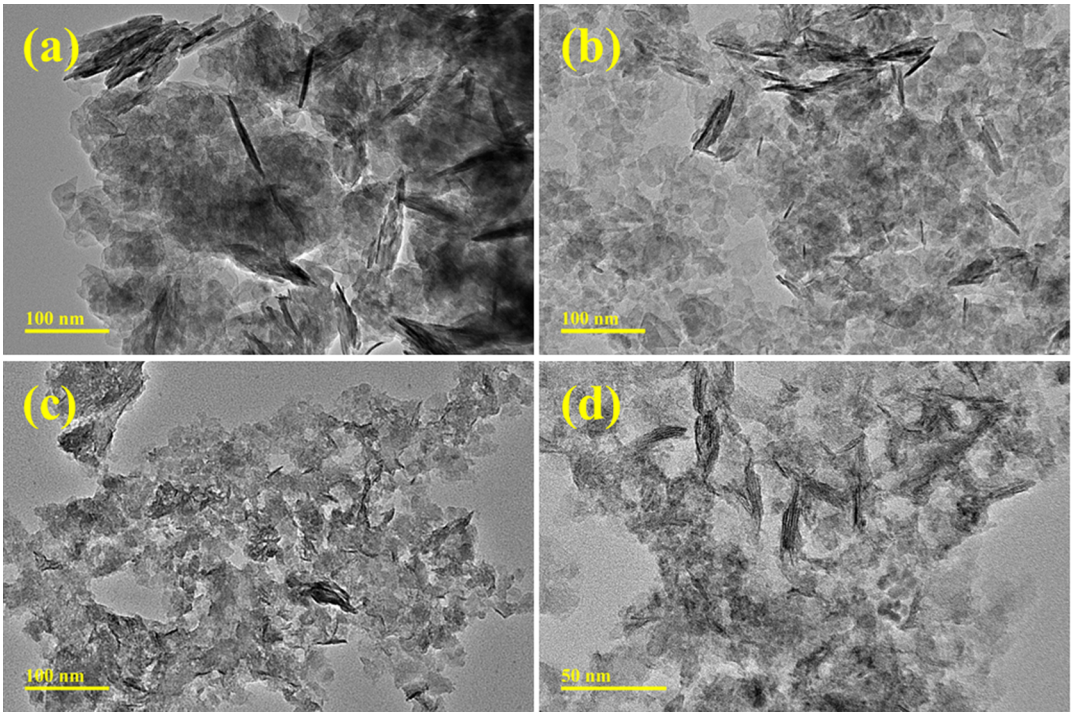

Figure 6. TEM micrographs of (a) NiO_2, (b) Cs-doped NiO_2, (c) (2 wt %) V_2O_5/Cs-doped NiO_2, and (d) (4 wt %) V_2O_5/Cs-doped NiO_2.

Since CA directly affects the production of H^+ ions in acidic media, the catalyst's surface becomes more positively charged. Since MB is also a cationic dye, its absorption is inhibited because catalyst surfaces are less receptive to the cationic adsorption of adsorbable families, which reduces the amount of dye that can be absorbed. This occurs due to the increased strength of the electrostatic repulsion force between the positively charged surfaces of the catalyst and the dye.[69,70] Generally, the catalyst's wide surface area or tiny size has provided more active sites to increase CA. Because of the microporosity, the catalyst's efficiency diminishes when the surface area is big because the reactant cannot diffuse into the binding sites of the catalyst.[71]

The well diffusion technique was followed to investigate the antibacterial activity observed in vitro, and the synthesized V_2O_5/Cs-NiO_2 NSs samples were tested for *E. coli* (Gram-negative bacteria) by measuring inhibition zones [49]. Significant inhibitory zones were seen against *E. coli* for

https://doi.org/10.1021/acsomega.3c00604
ACS Omega 2023, 8, 19474−19485

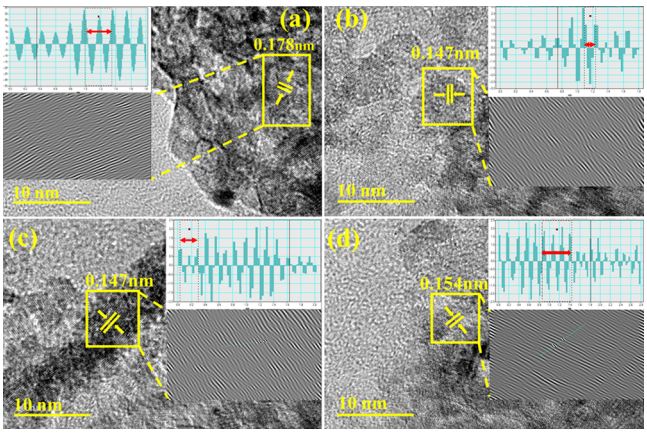

Figure 7. Interlayer d-spacing of (a) NiO_2, (b) Cs-doped NiO_2, (c) (2 wt %) V_2O_5/Cs-doped NiO_2, and (d) (4 wt %) V_2O_5/Cs-doped NiO_2.

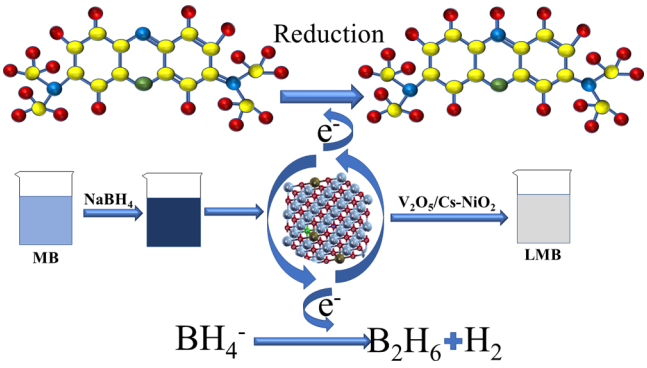

Figure 8. Schematic illustration of the catalytic reduction of dye in the presence of pristine and V_2O_5/Cs-doped NiO_2.

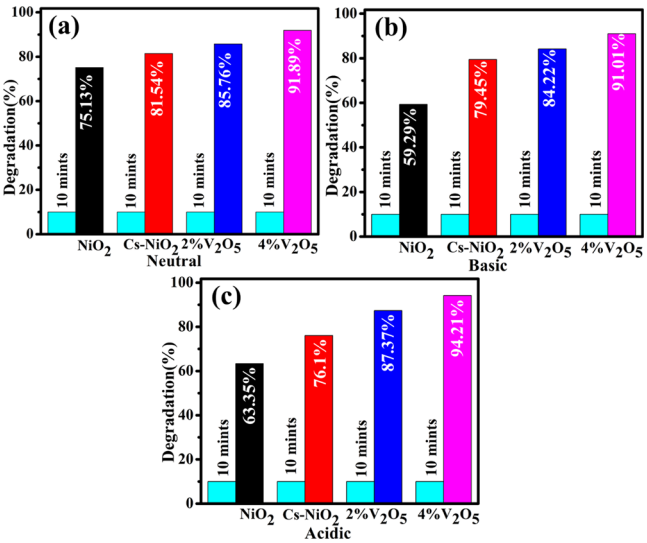

Figure 9. Catalytic potential of the pristine and (2 and 4 wt %) V_2O_5/Cs-doped NiO_2 in (a) neutral, (b) basic, and (c) acidic media.

doped and pure NSs, ranging from 1.30 to 3.05 mm in low and 2.25 to 3.75 mm in high concentrations, respectively, as exhibited in Table 2. All the observations were analyzed with ciprofloxacin at a concentration of 5.15 mm for Gram-negative bacteria and DI water at a concentration of 0 mm. At a concentration of 4 wt %, the V_2O_5/Cs-doped NiO_2 demonstrated an effective antibacterial action. As a result of the fact that since the doping concentration is directly related to the size of the inhibition zones, an enhancement in the measurements of the inhibition zones will naturally result in a higher doping concentration. *E. coli* showed a high antibacterial efficacy when it was in high concentrations. Table 3 shows the literature comparison for the antimicrobial activity of nickel oxide against *E. coli*.

The antibacterial activity was linked to a variety of parameters, including the size, shape, and concentration of the particles. Oxidative stress influences the phenotype, size, and mass-to-surface concentration of NSs. This is because nanoparticles quickly release ROS. ROS are responsible for degrading the cytoplasmic contents of the bacterial membrane, which ultimately leads to the death of the bacterium.[60] Since NiO_2 has a positive surface charge electrostatically attached to the negatively charged cell surface, it restricts cell activity.[75] The cell was left lifeless as a result of NiO_2 ability to enter the cell and its harmful effects that caused the death of bacteria. The preceding procedure is represented in Figure 10.

NSs connect themselves to the cell wall in the form of a helical, disorderly spring and enter the cell membrane, where they build interlinks with the structures of DNA molecules.[62] The effectiveness of the antimicrobial agent depends on the crystallite size and the doping concentration, and there is an inverse link between the size of the pure and the size of the V_2O_5/Cs-doped NiO_2 NSs. Because of their diminutive dimensions, the particles actively produce ROS, which, in turn, create a rupture in the bacterial cell membrane and the exposure of the bacterium's cytoplasmic components, which finally leads to the death of the bacterium. The mechanism for the generation of ROS performed under the presence of visible light can be exhibited as

$$NiO_2 + h\nu \text{ (visible light)} \rightarrow h^+ \text{ (hole)} + e^- \text{ (excited electron)}$$

$$e^- + O_2 \rightarrow {}^2O^{*-}$$

$$h^+ + H_2O \rightarrow OH^- + H^+$$

$${}^{-}O^*{}_2 + H^{+2}HO^*$$

$${}^2HO^* + e^- + H^+ \rightarrow {}^2H^*O_2$$

$${}^2H^*O_2 + {}^{-}O^*{}_2 \rightarrow O^*H + O_2 + OH^-$$

The mechanism for the response of antimicrobial activity is depicted in Figure 9, where ROS plays an effective part in the death of microbial agents.[76] Due to the direct attack of the synthesized materials, the cell wall and cell membrane of the bacteria are damaged, ultimately resulting in the death of the pathogen. NSs that generate intracellular ROS communicate with the nucleic acid of a bacterial cell, which causes single as well as dual-wrecked breakage within the nitrogen base and sugar-phosphate bond of nucleic acid.[59]

Drug resistance is seen as a serious threat to humanity, and there is a continuing need for effective antibiotics. Metal NSs are commonly believed to have a role in antibacterial activity. Trimethoprim and sulfonamide medicines are known to target the enzymes DHFR and DHPS in the folic acid production pathway.[77,78] Here, we tested Cs-doped NiO_2 and V_2O_5/Cs-doped NiO_2 for their ability to bind to the DHFR and DHPS

https://doi.org/10.1021/acsomega.3c00604
ACS Omega 2023, 8, 19474−19485

Table 1. Comparison for the Reduction/Degradation (Red/Deg) of MB from Literature and Current Research

nanocatalyst	size (nm)	synthesis method	dye	time (min)	Red/Deg (%)	under light/dark	ref
NiO/Ag heterostructure	25	hydrothermal	MB	210	70	light	65
NiO nanoparticles	2−5.4	thermal decomposition	RhB, MB	300	RhB: 87MB: 70	light	66
NiO-CuO nanoparticles	14−36	sol−gel	MB	26	40	light	67
NiO/ZnO composite	28.3	electrospinning	RhB, MB	180	RhB: 59.41MB: 65.43	light	68
Cu-doped CNC/NiO composite	19.1	co-precipitation	MB	30	70.6	dark	21
V_2O_5/Cs-NiO_2 NSs	45.19	co-precipitation	MB	10	94.21	dark	this work

Table 2. Antimicrobial Potential of NiO_2 and (2 and 4 wt %) V_2O_5/Cs-Doped NiO_2 NSs

	E. coli inhibition zone (mm)			
samples	0.5 mg/50 μL	1.0 mg/50 μL	ciprofloxacin	DI water
NiO_2	1.30	2.25	5.15	0
Cs-NiO_2	1.95	2.55	5.15	0
(2%) V_2O_5/Cs-NiO_2	2.15	3.05	5.15	0
(4%) V_2O_5/Cs-NiO_2	3.05	3.75	5.15	0

Table 3. Literature Comparison of Antimicrobial Activity of Nickel Oxide with the Current Study

sample	preparation method	pathogen	% of inhabitation zone	ref
graphene oxide-nickel oxide (GO-NiO) nanocomposite	hydrothermal	*E. coli*	0	72
NiO nanoparticles	green synthesis	*E. coli*	27.7	73
Cu-doped CNC/NiO nanocrystals	co-precipitation	*E. coli*	56.65	21
BC-Ag/NiO nanocomposite	hydrothermal	*E. coli*	57	74
V_2O_5/Cs-NiO_2 NSs	co-precipitation	*E. coli*	70	this work

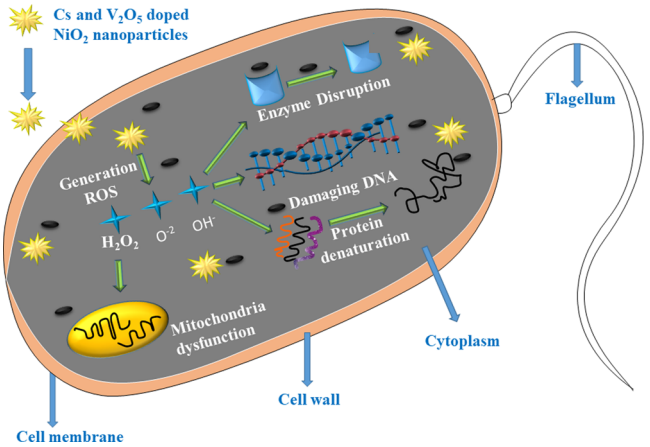

Figure 10. Antibacterial mechanism of produced NiO_2 and V_2O_5/Cs-doped NiO_2 schematically.

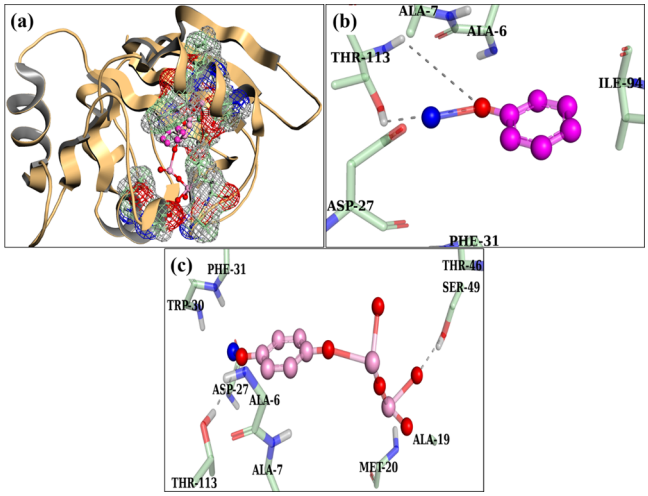

Figure 11. Binding pocket (a) and interaction pattern of Cs-doped NiO_2 (b) and V_2O_5/Cs-doped NiO_2 (c) inside active pocket DHFR from *E. coli*.

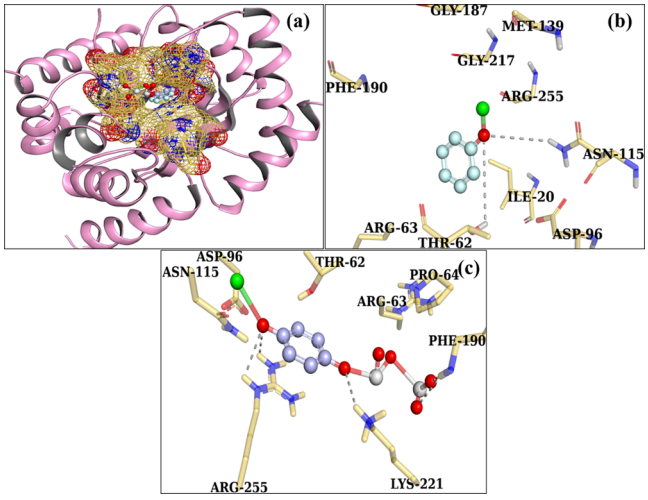

Figure 12. Binding pocket (a) and interaction pattern of Cs-doped NiO_2 (b) and V_2O_5/Cs-doped NiO_2 (c) inside active pocket DHPS from *E. coli*.

enzymes found in *E. coli*. Potential enzyme inhibitors were identified based on the binding pattern of docked complexes inside the active site of the target enzyme. The best docking zone for $DHFR_{E.coli}$ had H-bonding interactions with Ala-7 and Thr-113 for Cs-doped NiO_2 and Ser-49 and Thr-113 for V_2O_5/Cs-doped NiO_2, with binding scores of 3.28 and 6.37, respectively (Figure 11).

In Figure 12, the docking complex of Cs-doped NiO_2 for $DHPS_{E.coli}$ exhibited H-bonding with Thr-62 and Asn-115 having a docking score of 2.40. At the same time, V_2O_5/Cs-doped NiO_2 showed H-bonding with Phe-190, Lys-221, and Arg-255 with a binding energy of 4.31. These V_2O_5/Cs-doped NiO_2 NSs were proposed as potential antagonists. Enzyme activity stops when ligand binding prevents the substrate from entering the active site. In silico estimations for selective targets showed their potential binding patterns into the active

https://doi.org/10.1021/acsomega.3c00604
ACS Omega 2023, 8, 19474−19485

pocket of the enzyme and proposed those compounds as enzyme inhibitors. V_2O_5/Cs-doped NiO_2 NSs had an enhanced antibacterial action against *E. coli*.

4. CONCLUSIONS

The co-precipitation technique was used to synthesize the (2 and 4 wt %) V_2O_5/Cs-doped NiO_2 NSs. The XRD pattern verified the hexagonal crystal structures and SAED confirmed the polycrystalline nature of the synthesized NSs. The elemental composition and NSs morphology was confirmed by EDS and TEM micrographs. The synthesized NSs were examined as a catalyst for the degradation of MB and its antimicrobial activity against *E. coli*. The influence of Cs and V_2O_5 as dopants in NiO_2 results in a more efficient and effective catalyst. In principle, Cs provide a wide surface area and porous structure, and V_2O_5 generates more ROS and boosts the redox reactions. Hence, NiO_2 doped with (4 wt %) V_2O_5/Cs demonstrated a remarkable CA at 91.98, 91.01, and 94.21% in neutral, basic, and acidic media, respectively, against MB reduction. The high bactericidal effectiveness against *E. coli* with a measured inhibition zone of 3.75 mm at high concentration was observed. In addition, molecular docking analysis suggested that V_2O_5/Cs-doped NiO_2 NSs might block the DHFR and DHPS. This research concludes that (4 wt %) V_2O_5/Cs-doped NiO_2 is an efficient catalytic material for degrading dye and a worthy candidate for antibacterial activities. This study aims to provide new insight into developing a NiO_2-based catalyst for bioremediation and CA.

■ ASSOCIATED CONTENT

Data Availability Statement

On-demand accessibility to data is possible.

■ AUTHOR INFORMATION

Corresponding Authors

Muhammad Ikram − *Solar Cell Applications Research Lab, Department of Physics, Government College University Lahore, Lahore 54000 Punjab, Pakistan;* orcid.org/0000-0001-7741-789X; Email: dr.muhammadikram@gcu.edu.pk

Anwar Ul-Hamid − *Core Research Facilities, King Fahd University of Petroleum & Minerals, Dhahran 31261, Saudi Arabia;* orcid.org/0000-0002-0259-301X; Email: anwar@kfupm.edu.sa

Walid Nabgan − *Departament d'Enginyeria Química, Universitat Rovira i Virgili, 43007 Tarragona, Spain;* orcid.org/0000-0001-9901-862X; Email: walid.nabgan@urv.cat

Authors

Shair Baz − *Solar Cell Applications Research Lab, Department of Physics, Government College University Lahore, Lahore 54000 Punjab, Pakistan*

Ali Haider − *Department of Clinical Sciences, Faculty of Veterinary and Animal Sciences, Muhammad Nawaz Shareef, University of Agriculture, 66000 Multan, Punjab, Pakistan*

Anum Shahzadi − *Faculty of Pharmacy, The University of Lahore, Lahore 54000, Pakistan*

Junaid Haider − *Tianjin Institute of Industrial Biotechnology, Chinese Academy of Sciences, Tianjin 300308, China;* orcid.org/0000-0002-2254-1196

M. Imran − *Department of Chemistry, Government College University Faisalabad, Sahiwal, Punjab 57000, Pakistan*

Thamraa Alshahrani − *Department of Physics, College of Sciences, Princess Nourah bint Abdulrahman University (PNU), Riyadh 11671, Saudi Arabia*

Francisco Medina − *Departament d'Enginyeria Química, Universitat Rovira i Virgili, 43007 Tarragona, Spain;* orcid.org/0000-0002-3111-1542

Muhammad Imran − *Solar Cell Applications Research Lab, Department of Physics, Government College University Lahore, Lahore 54000 Punjab, Pakistan*

Complete contact information is available at: https://pubs.acs.org/10.1021/acsomega.3c00604

Funding

We would like to express our appreciation to the Higher Education Commission of Pakistan for funding project NRPU-20-17615 (Dr. M.I.).

Notes

The authors declare no competing financial interest.

■ ACKNOWLEDGMENTS

W.N. is thankful for the support from Universitat Rovira i Virgili under the Maria Zambrano Programme (reference number: 2021URV-MZ-10), Proyectos de Generación de Conocimiento AEI/MCIN (PID2021-123665OB-I00), and the project reference number of TED2021−129343B-I00. This research was funded by the Princess Nourah bint Abdulrahman University Researchers Supporting Project number (PNURSP2023R1), Princess Nourah bint Abdulrahman University, Riyadh, Saudi Arabia. Authors are also thankful for the support from Grant PID2021-123665OB-I00 and TED2021-129343B-I00 funded by MCIN/AEI/10.13039/501100011033 and, as appropriate, by "ERDF A way of making Europe", by the "European Union" or by the "European Union NextGenerationEU/PRTR".

■ REFERENCES

(1) Kookana, R. S.; Drechsel, P.; Jamwal, P.; Vanderzalm, J. Urbanisation and emerging economies: Issues and potential solutions for water and food security. *Sci. Total Environ.* **2020**, *732*, No. 139057.

(2) Yang, J.; Shojaei, S.; Shojaei, S. Removal of drug and dye from aqueous solutions by graphene oxide: Adsorption studies and chemometrics methods. *npj Clean. Water* **2022**, *5*, 5.

(3) Islam, A.; Teo, S. H.; Taufiq-Yap, Y. H.; Ng, C. H.; Vo, D.-V. N.; Ibrahim, M. L.; Hasan, M. M.; Khan, M. A. R.; Nur, A. S. M.; Awual, M. R. Step towards the sustainable toxic dyes removal and recycling from aqueous solution- A comprehensive review. *Resour., Conserv. Recycl.* **2021**, *175*, No. 105849.

(4) Ikram, M.; Haider, A.; Imran, M.; Haider, J.; Ul-Hamid, A.; Shahzadi, A.; Malik, R.; Nabgan, W.; Nazir, G.; Ali, S. Graphitic-C_3N_4/chitosan-doped NiO nanostructure to treat the polluted water and their bactericidal with in silico molecular docking analysis. *Int. J. Biol. Macromol.* **2022**, *277*, 962−973.

(5) Santoso, S. P.; Bundjaja, V.; Angkawijaya, A. E.; Gunarto, C.; Go, A. W.; Yuliana, M.; Tran-Nguyen, P. L.; Hsieh, C.-W.; Ju, Y.-H. One-step synthesis of nitrogen-grafted copper-gallic acid for enhanced methylene blue removal. *Sci. Rep.* **2021**, *11*, 12021.

(6) Ali, M.; Sharif, S.; Anjum, S.; Imran, M.; Ikram, M.; Naz, M.; Ali, S. Preparation of Co and Ni doped ZnO nanoparticles served as encouraging nano-catalytic application. *Mater. Res. Express* **2019**, *6*, 1250d5.

(7) Vázquez-Cuchillo, O.; Cruz-López, A.; Bautista-Carrillo, L. M.; Bautista-Hernández, A.; Torres Martínez, L. M.; Wohn Lee, S.

Synthesis of TiO_2 using different hydrolysis catalysts and doped with Zn for efficient degradation of aqueous phase pollutants under UV light. *Res. Chem. Intermed.* **2010**, *36*, 103−113.
(8) Thennarasu, G.; Sivasamy, A. Enhanced visible photocatalytic activity of cotton ball like nano structured Cu doped ZnO for the degradation of organic pollutant. *Ecotoxicol. Environ. Saf.* **2016**, *134*, 412−420.
(9) Liu, F.; Yang, J.; Zuo, J.; Ma, D.; Gan, L.; Xie, B.; Wang, P.; Yang, B. Graphene-supported nanoscale zero-valent iron: Removal of phosphorus from aqueous solution and mechanistic study. *J. Environ. Sci.* **2014**, *26*, 1751−1762.
(10) Balusamy, B.; Kandhasamy, Y. G.; Senthamizhan, A.; Chandrasekaran, G.; Subramanian, M. S.; Kumaravel, T. S. Characterization and bacterial toxicity of lanthanum oxide bulk and nanoparticles. *J. Rare Earths* **2012**, *30*, 1298−1302.
(11) Phung, T. H.; Srinivasan, D. K.; Steinmann, P.; Wise, R.; Yu, M.-B.; Yeo, Y.-C.; Chunxiang, Z. High performance metal-insulator-metal capacitors with Er2O3 on ALD SiO2 for RF applications. *J. Electrochem. Soc.* **2011**, *158*, H1289.
(12) Wang, J.; Ji, T.; Zhu, Y.; Fang, Z.; Ren, W. Band gap and structure characterization of Tm_2O_3 films. *J. Rare Earths* **2012**, *30*, 233−235.
(13) Mudavakkat, V. H.; Atuchin, V. V.; Kruchinin, V. N.; Kayani, A.; Ramana, C. V. Structure, morphology and optical properties of nanocrystalline yttrium oxide (Y_2O_3) thin films. *Opt. Mater.* **2012**, *34*, 893−900.
(14) Rahdar, A.; Aliahmad, M.; Azizi, Y. NiO nanoparticles: synthesis and characterization. *J. Nanostruct.* **2015**, *5*, 145−151.
(15) Hameeda, B.; Mushtaq, A.; Saeed, M.; Munir, A.; Jabeen, U.; Waseem, A. Development of Cu-doped NiO nanoscale material as efficient photocatalyst for visible light dye degradation. *Toxin Rev.* **2021**, *40*, 1396−1406.
(16) Ajitha, B.; Ahn, C. W.; Yadav, P. V. K.; Reddy, Y. A. K. Silver nanoparticle embedded polymethacrylic acid/ polyvinylpyrrolidone nanofibers for catalytic application. *J. Environ. Chem. Eng.* **2021**, *9*, No. 106291.
(17) Jamil, S.; Ahmad, Z.; Ali, M.; Rauf Khan, S.; Ali, S.; Amen Hammami, M.; Haroon, M.; Saleh, T. A.; Janjua, R. S. A. M. Synthesis and characterization of polyaniline/nickel oxide composites for fuel additive and dyes reduction. *Chem. Phys. Lett.* **2021**, *776*, No. 138713.
(18) Lu, J.; Fang, J.; Li, J.; Wang, C.; He, Z.; Zhu, L.; Xu, Z.; Zeng, H. Polydopamine Nanotubes Decorated with Ag Nanoparticles as Catalyst for the Reduction of Methylene Blue. *ACS Appl. Nano Mater.* **2020**, *3*, 156−164.
(19) Ambreen, J.; Al-Harbi, F. F.; Sakhawat, H.; Ajmal, M.; Naeem, H.; Farooqi, Z. H.; Batool, N.; Siddiq, M. Fabrication of poly (N-vinylcaprolactam-co-acrylic acid)-silver nanoparticles composite microgel with substantial potential of hydrogen peroxide sensing and catalyzing the reduction of water pollutants. *J. Mol. Liq.* **2022**, *355*, No. 118931.
(20) Hu, Z.; Han, M.; Chen, C.; Zou, Z.; Shen, Y.; Fu, Z.; Zhu, X.; Zhang, Y.; Zhang, H.; Zhao, H.; et al. Hollow carbon sphere encapsulated nickel nanoreactor for aqueous-phase hydrogenation-rearrangement tandem reaction with enhanced catalytic performance. *Appl. Catal., B* **2022**, *306*, No. 121140.
(21) Ikram, M.; Bashir, Z.; Haider, A.; Naz, S.; Ul-Hamid, A.; Shahzadi, I.; Ashfaq, A.; Haider, J.; Shahzadi, A.; Ali, S. Bactericidal action and molecular docking studies of catalytic Cu-doped NiO composited with cellulose nanocrystals. *Int. J. Biol. Macromol.* **2022**, *195*, 440−448.
(22) Iqbal, S.; Javed, M.; Bahadur, A.; Qamar, M.; Ahmad, M.; Shoaib, M.; Raheel, M.; Ahmed, N.; Akbar, M. B.; Li, H. Controlled synthesis of Ag-doped CuO nanoparticles as a core with poly(acrylic acid) microgel shell for efficient removal of methylene blue under visible light. *J. Mater. Sci.: Mater. Electron.* **2020**, *31*, 8423−8435.
(23) Nandana, C. N.; Christeena, M.; Bharathi, D. Synthesis and characterization of chitosan/silver nanocomposite using rutin for antibacterial, antioxidant and photocatalytic applications. *J. Cluster Sci.* **2021**, *33*, 269−279.
(24) Dou, J.; Yin, S.; Chong, J. Y.; Zhang, B.; Han, J.; Huang, Y.; Xu, R. Carbon spheres anchored Co_3O_4 nanoclusters as an efficient catalyst for dye degradation. *Appl. Catal., A* **2016**, *513*, 106−115.
(25) Cheng, X.; Fu, A.; Li, H.; Wang, Y.; Guo, P.; Liu, J.; Zhang, J.; Zhao, X. S. Sustainable Preparation of Copper Particles Decorated Carbon Microspheres and Studies on Their Bactericidal Activity and Catalytic Properties. *ACS Sustainable Chem. Eng.* **2015**, *3*, 2414−2422.
(26) Jin, Q.; Shen, Y.; Cai, Y.; Chu, L.; Zeng, Y. Resource utilization of waste V2O5-based deNOx catalysts for hydrogen production from formaldehyde and water via steam reforming. *J. Hazard. Mater.* **2020**, *381*, No. 120934.
(27) Levi, R.; Bar-Sadan, M.; Albu-Yaron, A.; Popovitz-Biro, R.; Houben, L.; Shahar, C.; Enyashin, A.; Seifert, G.; Prior, Y.; Tenne, R. Hollow V2O5 Nanoparticles (Fullerene-Like Analogues) Prepared by Laser Ablation. *J. Am. Chem. Soc.* **2010**, *132*, 11214−11222.
(28) Babar, B. M.; Pisal, K. B.; Sutar, S. H.; Mujawar, S. H.; Kadam, L. D.; Pathan, H. M.; Pawar, U. T.; Kadam, P. M.; Patil, P. S. Hydrothermally Prepared Vanadium Oxide Nanostructures for Photocatalytic Application. *ES Energy Environ.* **2022**, *15*, 82−91.
(29) Santosham, M.; Chandran, A.; Fitzwater, S.; Fischer-Walker, C.; Baqui, A. H.; Black, R. Progress and barriers for the control of diarrhoeal disease. *Lancet* **2010**, *376*, 63−67.
(30) Xiang, Q.; Yu, J.; Jaroniec, M. Graphene-based semiconductor photocatalysts. *Chem. Soc. Rev.* **2012**, *41*, 782−796.
(31) Bhimanapati, G. R.; Lin, Z.; Meunier, V.; Jung, Y.; Cha, J.; Das, S.; Xiao, D.; Son, Y.; Strano, M. S.; Cooper, V. R.; et al. Recent Advances in Two-Dimensional Materials beyond Graphene. *ACS Nano* **2015**, *9*, 11509−11539.
(32) Bergey, D.; JG, H. *Bergey's Manual of Determinative Bacteriology. Baltimore*. 9th ed; Williams and Wilkins: USA. 1994.
(33) Bauer, A. Antibiotic susceptibility testing by a standardized single disc method. *Am. J. Clin. Pathol.* **1966**, *45*, 149−158.
(34) Adzitey, F.; Yussif, S.; Ayamga, R.; Zuberu, S.; Addy, F.; Adu-Bonsu, G.; Huda, N.; Kobun, R. Antimicrobial susceptibility and molecular characterization of Escherichia coli recovered from milk and related samples. *Microorganisms* **2022**, *10*, 1335.
(35) Vijay, S.; Sharma, M.; Misri, J.; Shome, B.; Veeraraghavan, B.; Ray, P.; Ohri, V.; Walia, K. An integrated surveillance network for antimicrobial resistance, India. *Bull. W. H. O.* **2021**, *99*, 562.
(36) Iwalokun, B.; Ogunledun, A.; Ogbolu, D.; Bamiro, S.; Jimi-Omojola, J. In vitro antimicrobial properties of aqueous garlic extract against multidrug-resistant bacteria and Candida species from Nigeria. *J. Med. Food* **2004**, *7*, 327−333.
(37) Haider, A.; Ijaz, M.; Imran, M.; Naz, M.; Majeed, H.; Khan, J. A.; Ali, M. M.; Ikram, M. Enhanced bactericidal action and dye degradation of spicy roots' extract-incorporated fine-tuned metal oxide nanoparticles. *Appl. Nanosci.* **2020**, *10*, 1095−1104.
(38) Haider, A.; Ijaz, M.; Ali, S.; Haider, J.; Imran, M.; Majeed, H.; Shahzadi, I.; Ali, M. M.; Khan, J. A.; Ikram, M. Green Synthesized Phytochemically (Zingiber officinale and Allium sativum) Reduced Nickel Oxide Nanoparticles Confirmed Bactericidal and Catalytic Potential. *Nanoscale Res. Lett.* **2020**, *15*, 50.
(39) Summerfield, R. L.; Daigle, D. M.; Mayer, S.; Mallik, D.; Hughes, D. W.; Jackson, S. G.; Sulek, M.; Organ, M. G.; Brown, E. D.; Junop, M. S. A 2.13 Å Structure of E. coli Dihydrofolate Reductase Bound to a Novel Competitive Inhibitor Reveals a New Binding Surface Involving the M20 Loop Region. *J. Med. Chem.* **2006**, *49*, 6977−6986.
(40) Dennis, M. L.; Lee, M. D.; Harjani, J. R.; Ahmed, M.; DeBono, A. J.; Pitcher, N. P.; Wang, Z.-C.; Chhabra, S.; Barlow, N.; Rahmani, R.; et al. 8-Mercaptoguanine Derivatives as Inhibitors of Dihydropteroate Synthase. *Chem. − Eur. J.* **2018**, *24*, 1922−1930.
(41) Ikram, M.; Chaudhary, K.; Shahzadi, A.; Haider, A.; Shahzadi, I.; Ul-Hamid, A.; Abid, N.; Haider, J.; Nabgan, W.; Butt, A. R. Chitosan/starch-doped MnO2 nanocomposite served as dye degradation, bacterial activity, and insilico molecular docking study. *Mater. Today Nano* **2022**, *20*, No. 100271.
(42) Shahzadi, I.; Islam, M.; Saeed, H.; Haider, A.; Shahzadi, A.; Haider, J.; Ahmed, N.; Ul-Hamid, A.; Nabgan, W.; Ikram, M.; et al.

https://doi.org/10.1021/acsomega.3c00604
ACS Omega 2023, 8, 19474−19485

Formation of biocompatible MgO/cellulose grafted hydrogel for efficient bactericidal and controlled release of doxorubicin. *Int. J. Biol. Macromol.* **2022**, *220*, 1277−1286.
(43) Abd-Alghafour, N.; Ahmed, N. M.; Hassan, Z.; Almessiere, M. A. In *Hydrothermal synthesis and structural properties of V2O5 Nanoflowers at low temperatures. J. Phys.: Conf. Ser.* **2018**, *1083*, No. 012036.
(44) Hu, L.; Peng, J.; Wang, W.; Xia, Z.; Yuan, J.; Lu, J.; Huang, X.; Ma, W.; Song, H.; Chen, W.; et al. Sequential Deposition of CH3NH3PbI3 on Planar NiO Film for Efficient Planar Perovskite Solar Cells. *ACS Photonics* **2014**, *1*, 547−553.
(45) Anand, K.; Kaur, J.; Singh, R. C.; Thangaraj, R. Preparation and characterization of Ag-doped In2O3 nanoparticles gas sensor. *Chem. Phys. Lett.* **2017**, *682*, 140−146.
(46) Yuan, X.; Zhou, C.; Jing, Q.; Tang, Q.; Mu, Y.; du, A. K. Facile synthesis of g-C3N4 nanosheets/ZnO nanocomposites with enhanced photocatalytic activity in reduction of aqueous chromium (VI) under visible light. *Nanomaterials* **2016**, *6*, 173.
(47) Susha, N.; Nandakumar, K.; Nair, S. S. Enhanced photoconductivity in CdS/betanin composite nanostructures. *RSC Adv.* **2018**, *8*, 11330−11337.
(48) Khairnar, S. D.; Shrivastava, V. S. Facile synthesis of nickel oxide nanoparticles for the degradation of Methylene blue and Rhodamine B dye: a comparative study. *Journal of Taibah University for Science* **2019**, *13*, 1108−1118.
(49) López-Ortiz, A.; Collins-Martínez, V. H.; Hernández-Escobar, C. A.; Flores-Gallardo, S. G.; Zaragoza-Contreras, E. A. Protection of NiO nanoparticles against leaching in acid medium by grafting of polyacrylic acid. *Mater. Chem. Phys.* **2008**, *109*, 306−310.
(50) Yousaf, S.; Zulfiqar, S.; Shahi, M. N.; Warsi, M. F.; Al-Khalli, N. F.; Aly Aboud, M. F.; Shakir, I. Tuning the structural, optical and electrical properties of NiO nanoparticles prepared by wet chemical route. *Ceram. Int.* **2020**, *46*, 3750−3758.
(51) Ngo, Y.-L. T.; Hur, S. H. Low-temperature NO2 gas sensor fabricated with NiO and reduced graphene oxide hybrid structure. *Mater. Res. Bull.* **2016**, *84*, 168−176.
(52) Wei, Z.; Qiao, H.; Yang, H.; Zhang, C.; Yan, X. Characterization of NiO nanoparticles by anodic arc plasma method. *J. Alloys Compd.* **2009**, *479*, 855−858.
(53) Barzinjy, A. A.; Hamad, S. M.; Aydın, S.; Ahmed, M. H.; Hussain, F. H. S. Green and eco-friendly synthesis of Nickel oxide nanoparticles and its photocatalytic activity for methyl orange degradation. *J. Mater. Sci.: Mater. Electron.* **2020**, *31*, 11303−11316.
(54) Barakat, A.; Al-Noaimi, M.; Suleiman, M.; Aldwayyan, A. S.; Hammouti, B.; Ben Hadda, T.; Haddad, S. F.; Boshaala, A.; Warad, I. One step synthesis of NiO nanoparticles via solid-state thermal decomposition at low-temperature of novel aqua (2, 9-dimethyl-1, 10-phenanthroline) NiCl2 complex. *Int. J. Mol. Sci.* **2013**, *14*, 23941−23954.
(55) Hazeghi, F.; Mozaffari, S.; Ghorashi, S. M. B. Metal organic framework−derived core-shell CuO@NiO nanosphares as hole transport material in perovskite solar cell. *J. Solid State Electrochem.* **2020**, *24*, 1427−1438.
(56) Reddy, B. R.; Harish, G.; Reddy, C. S.; Reddy, P. S. Synthesis and characterization of Cu doped NiO nanoparticles. *Int. J. Mod. Eng. Res.* **2014**, *4*, 62−66.
(57) Adeleye, A. S.; Conway, J. R.; Garner, K.; Huang, Y.; Su, Y.; Keller, A. A. Engineered nanomaterials for water treatment and remediation: Costs, benefits, and applicability. *Chem. Eng. J.* **2016**, *286*, 640−662.
(58) Mafa, P. J.; Mamba, B. B.; Kuvarega, A. T. Construction of hierarchical BiPW12O40/BiOI p−n heterojunction with enhanced visible light activity for degradation of endocrine disrupting Bisphenol A. *Sep. Purif. Technol.* **2020**, *253*, No. 117349.
(59) Mustajab, M.; Ikram, M.; Haider, A.; Ul-Hamid, A.; Nabgan, W.; Haider, J.; Ghaffar, R.; Shahzadi, A.; Ghaffar, A.; Saeed, A. Promising performance of polyvinylpyrrolidone-doped bismuth oxyiodide quantum dots for antibacterial and catalytic applications. *Appl. Nanosci.* **2022**, *12*, 2621−2633.
(60) Khan, A. D.; Ikram, M.; Haider, A.; Ul-Hamid, A.; Nabgan, W.; Haider, J. Polyvinylpyrrolidone and chitosan-doped lanthanum oxide nanostructures used as anti-bacterial agents and nano-catalyst. *Appl. Nanosci.* **2022**, *12*, 2227−2239.
(61) Anjana, R.; Geetha, N. Degradation Of Methylene Blue using Silver Nanoparticles Synthesized from Cynodon dactylon (L.) Pers. Leaf aqueous extract. *Int. J. Sci. Technol. Res.* **2019**, *8*, 225−229.
(62) Ikram, M.; Inayat, T.; Haider, A.; Ul-Hamid, A.; Haider, J.; Nabgan, W.; Saeed, A.; Shahbaz, A.; Hayat, S.; Ul-Ain, K.; et al. Graphene Oxide-Doped MgO Nanostructures for Highly Efficient Dye Degradation and Bactericidal Action. *Nanoscale Res. Lett.* **2021**, *16*, 56.
(63) Bari, A.; Ikram, M.; Haider, A.; Ul-Hamid, A.; Haider, J.; Shahzadi, I.; Nazir, G.; Shahzadi, A.; Imran, M.; Ghaffar, A. Evaluation of bactericidal potential and catalytic dye degradation of multiple morphology based chitosan/polyvinylpyrrolidone-doped bismuth oxide nanostructures. *Nanoscale Adv.* **2022**, *4*, 2713−2728.
(64) Moeen, S.; Ikram, M.; Haider, A.; Haider, J.; Ul-Hamid, A.; Nabgan, W.; Shujah, T.; Naz, M.; Shahzadi, I. Comparative Study of Sonophotocatalytic, Photocatalytic, and Catalytic Activities of Magnesium and Chitosan-Doped Tin Oxide Quantum Dots. *ACS Omega* **2022**, *7*, 46428−46439.
(65) Majumder, S.; Bhattacharjee, S.; Ghosh, C. K. NiO/Ag heterostructure: enhanced UV emission intensity, exchange interaction and photocatalytic activity. *RSC Adv.* **2016**, *6*, 56503−56510.
(66) Ramesh, M.; Rao, M. P. C.; Anandan, S.; Nagaraja, H. Adsorption and photocatalytic properties of NiO nanoparticles synthesized via a thermal decomposition process. *J. Mater. Res.* **2018**, *33*, 601−610.
(67) Senobari, S.; Nezamzadeh-Ejhieh, A. A comprehensive study on the enhanced photocatalytic activity of CuO-NiO nanoparticles: designing the experiments. *J. Mol. Liq.* **2018**, *261*, 208−217.
(68) Sabzehmeidani, M. M.; Karimi, H.; Ghaedi, M. Electrospinning preparation of NiO/ZnO composite nanofibers for photodegradation of binary mixture of rhodamine B and methylene blue in aqueous solution: central composite optimization. *Appl. Organomet. Chem.* **2018**, *32*, No. e4335.
(69) Singh, K. P.; Mohan, D.; Sinha, S.; Tondon, G. S.; Gosh, D. Color Removal from Wastewater Using Low-Cost Activated Carbon Derived from Agricultural Waste Material. *Ind. Eng. Chem. Res.* **2003**, *42*, 1965−1976.
(70) Haque, E.; Jun, J. W.; Jhung, S. H. Adsorptive removal of methyl orange and methylene blue from aqueous solution with a metal-organic framework material, iron terephthalate (MOF-235). *J. Hazard. Mater.* **2011**, *185*, 507−511.
(71) Ikram, M.; Hayat, S.; Imran, M.; Haider, A.; Naz, S.; Ul-Hamid, A.; Shahzadi, I.; Haider, J.; Shahzadi, A.; Nabgan, W.; et al. Novel Ag/cellulose-doped CeO2 quantum dots for efficient dye degradation and bactericidal activity with molecular docking study. *Carbohydr. Polym.* **2021**, *269*, No. 118346.
(72) Archana, S.; Jayanna, B. K.; Ananda, A.; Shilpa, B. M.; Pandiarajan, D.; Muralidhara, H. B.; Kumar, K. Y. Synthesis of nickel oxide grafted graphene oxide nanocomposites - A systematic research on chemisorption of heavy metal ions and its antibacterial activity. *Environ. Nanotechnol., Monit. Manage.* **2021**, *16*, No. 100486.
(73) Khodair, Z. T.; Ibrahim, N. M.; Kadhim, T. J.; Mohammad, A. M. Synthesis and characterization of nickel oxide (NiO) nanoparticles using an environmentally friendly method, and their biomedical applications. *Chem. Phys. Lett.* **2022**, *797*, No. 139564.
(74) Kamal, T.; Khalil, A.; Bakhsh, E. M.; Khan, S. B.; Chani, M. T. S.; Ul-Islam, M. Efficient fabrication, antibacterial and catalytic performance of Ag-NiO loaded bacterial cellulose paper. *Int. J. Biol. Macromol.* **2022**, *206*, 917−926.
(75) Rakshit, S.; Ghosh, S.; Chall, S.; Mati, S. S.; Moulik, S. P.; Bhattacharya, S. C. Controlled synthesis of spin glass nickel oxide nanoparticles and evaluation of their potential antimicrobial activity: A cost effective and eco friendly approach. *RSC Adv.* **2013**, *3*, 19348−19356.

https://doi.org/10.1021/acsomega.3c00604
ACS Omega 2023, 8, 19474−19485

(76) Ikram, M.; Haider, A.; Imran, M.; Haider, J.; Naz, S.; Ul-Hamid, A.; Nabgan, W.; Mustajab, M.; Shahzadi, A.; Shahzadi, I.; et al. Facile synthesis of starch and tellurium doped SrO nanocomposite for catalytic and antibacterial potential: In silico molecular docking studies. *Int. J. Biol. Macromol.* **2022**, *221*, 496−507.
(77) Ikram, M.; Abbasi, S.; Haider, A.; Naz, S.; Ul-Hamid, A.; Imran, M.; Haider, J.; Ghaffar, A. Bimetallic Ag/Cu incorporated into chemically exfoliated MoS2 nanosheets to enhance its antibacterial potential: in silico molecular docking studies. *Nanotechnology* **2020**, *31*, No. 275704.
(78) Hawser, S.; Lociuro, S.; Islam, K. Dihydrofolate reductase inhibitors as antibacterial agents. *Biochem. Pharmacol.* **2006**, *71*, 941−948.

https://doi.org/10.1021/acsomega.3c00604
ACS Omega 2023, 8, 19474−19485